Longwave infrared (LWIR) coded aperture dispersive spectrometer

C. Fernandez[1], B. D. Guenther[1], M. E. Gehm[1], D. J. Brady[1] and M. E. Sullivan[2]

1 Duke University,
Fitzpatrick Institute for Photonics and Department of Electrical and Computer Engineering,
Box 90291, Durham, NC 27708

2 Centice Corp, 215 Southport Dr,
Suite 1000, Morrisville, NC 27560
caf11@duke.edu

Abstract: We describe a static aperture-coded, dispersive longwave infrared (LWIR) spectrometer that uses a microbolometer array at the detector plane. The two-dimensional aperture code is based on a row-doubled Hadamard mask with transmissive and opaque openings. The independent column code nature of the matrix makes for a mathematically well-defined pattern that spatially and spectrally maps the source information to the detector plane. Post-processing techniques on the data provide spectral estimates of the source. Comparative experimental results between a slit and coded aperture for emission spectroscopy from a CO_2 laser are demonstrated.

OCIS codes: (120.0120) Instrumentation; (220.0220) Optical design and fabrication; (230.0230) Optical device; (300.6340) Infrared Spectroscopy.

References and links

1. S. C. Bates, P. W. M. Jr., and P. R. Solomon, "Infrared Monitoring of Combustion," in *SPIE*, Vol. 1434 (1991).
2. P. Jacquinot, "New developments in interference spectroscopy," Rep. Prog. Phys. **23**, 267–312 (1960).
3. P. Fellgett, "The Multiplex Advantage," Ph.D. thesis, Cambridge, UK (1951).
4. E. C. Cull, M. E. Gehm, and D. Brady, "Dispersion multiplexing with broadband filtering for miniature spectrometers," Appl. Opt. **46**, 365–374 (2007)
5. S. T. McCain, M. E. Gehm, Y. Wang, N. P. Pitsianis, and D. J. Brady, "Coded aperture Raman spectroscopy for quantitative measurements of ethanol in a tissue phantom solution," Appl. Spectrosc. **60**, 663–671 (2006).
6. M. E. Gehm, S. T. McCain, N. P. Pitsianis, D. J. Brady, P. Potuluri, and M. E. Sullivan, "Static two-dimensional aperture coding for multimodal, multiplex spectroscopy," Appl. Opt. **45**, 2965–2974 (2006).
7. T. Schimert, D. Ratcliff, J. Brady, S. Ropson, R. Gooch, B. Ritchey, P. McCardel, K. Rachels, M. Wand, M. Weinstein, and J. Wynn, "Low Cost, Low Power Uncooled a-Si-based Micro Infrared Camera for Unattended Ground Sensor Applications," in *SPIE Proceedings on Unattended Ground Sensor Technologies and Applications*, vol. 3713, pp. 101–111 (1999).
8. P. Richards, "Bolometers for infrared and millimeter waves," J. Appl. Phys. **76**, 1–24 (1994).
9. T. Schimert, N. Cunningham, G. Francisco, R. Gooch, J. Gooden, P. McCardel, B. Neal, B. Ritchey, J. Rife, A. J. Syllaios, J. Tregilgas, J. Brady, J. Gilstrap, and S. Ropson, "Low Cost, Low Power Uncooled 120x160 a-Si-based Micro Infrared Camera for Law Enforcement Applications," in *Proceedings of SPIE - The International Society for Optical Engineering*, vol. 4232, pp. 187–194 (2001).
10. R. G. Driggers, P. Cox, and T. Edwards, *Introduction to Infrared and Electro-Optical Systems* (Artech House, London, 1999).
11. G. Nitzsche and R. Riesenberg, "Noise, Fluctuation and HADAMARD-Transform-Spectrometry," in *Proceedings of SPIE Fluctuations and Noise in Photonics and Quantum Optics*, vol. 5111, pp. 273–282 (2003).
12. N. Menn, *Practical Optics* (Elsevier Academic Press, New York, 2004).

#78809 - $15.00 USD Received 10 Jan 2007; revised 20 Apr 2007; accepted 23 Apr 2007; published 25 Apr 2007

13. J. R. Wilson, *Handbook of Optics*, 2nd ed. (McGraw-Hill, Inc., 1995) Vol. 1.
14. C. L. Lawson and R. J. Hanson, *Solving Least Squares Problems* (Prentice-Hall, Inc, 1974).

1. Introduction

Infrared spectroscopy (IR) is popular for chemical detection because it provides the specificity necessary for the identification of organic and organometallic molecules found in many trace gases. It also provides complementary specificity to Raman spectroscopy without the associated low photon-efficiency. Previous studies in the longwave infrared region include absorption, emission and reflection spectroscopy with Fourier Transform Infrared (FTIR) systems. Some FTIR systems have been used to measure atmospheric pollutant gases from urban or agricultural sites. [1] Traditionally, FTIR based spectrometers are known for their high throughput (*Jacquinot*) advantage [2] and multiplex (*Fellgett*) advantage. [3] FTIR systems, while photon-efficient, typically contain movable parts that increase the cost of the system and increase data acquisition times. Dispersive systems exist, but lack the photon-efficiency obtained with FTIR systems. Unlike FTIR systems, dispersive spectrometers can contain no moving parts. We have been involved in the development of various coded aperture spectrometers for applications ranging from remote sensing [4] to biomedical applications. [5] Our systems replace the input slit of conventional dispersive spectrometer with a static 2-D aperture pattern mathematically well-conditioned for inversion. [6] The static 2-D aperture pattern used for the LWIR prototype is a row-doubled Hadamard matrix that has N/2 transmissive openings, where N is the order of the Hadamard matrix indicating the number of columns of the matrix. The aperture coded input in our LWIR prototype provides a spatial and spectral mapping of the source distribution at the heat sensitive detector plane. A mask-based dispersive spectrometer provides both the *Jacquinot* and *Fellgett* advantages exhibited by the FTIR spectrometer without the time delay or high cost associated with moving parts.

Over the last few years, the military has demanded low cost, low power, small imaging infrared camera surveillance in unattended ground sensor arrays. [7] Uncooled IR or thermal detectors have become of great interest for applications in the longwave infrared region. They provide a lightweight, low cost and low power solution to cooled photon detectors. In comparison to photon detectors, thermal detectors are sensitive over all wavelengths. Filters are commonly used to limit the spectral response of the detector . Types of thermal detectors include bolometers and pyroelectric arrays. We provided a spatial and spectral mapping at the input to the LWIR prototype for adequate spectral decomposition of the signal detected at the bolometer in the setup.

Bolometers, first developed by Langley[8], are characterized by the large temperature dependence of their resistivity. When photons, in the form of heat, are incident on the detector material the temperature rises and the resistance changes. Change in temperature and/or resistance is a measure of the intensity of the incident radiation. Amorphous silicon and vanadium oxide are typically used in bolometers for their high thermal coefficients of resistance.[9] A bolometer transforms an optical signal captured at the detector plane into a temperature and electrical change. Energy absorbed by the detector material increases the temperature of the material in the bolometer. [10] The electrical output of the detector is proportional to the incident optical power on the detector plane. Noise sources for bolometers, however, present challenges that affect complete restoration of the source from the input plane. Noise sources include pattern noise, photon noise, Johnson noise, and 1/f (flicker) noise.

Here we apply ideas from previously developed coded aperture spectrometers to LWIR emission spectroscopy. In this paper, we describe a first proof of concept system that uses a microbolometer at the focal plane. We report results obtained with an extended source from a tunable CO_2 laser incident at the input to an aperture-coded dispersive spectrometer using a

#78809 - $15.00 USD Received 10 Jan 2007; revised 20 Apr 2007; accepted 23 Apr 2007; published 25 Apr 2007

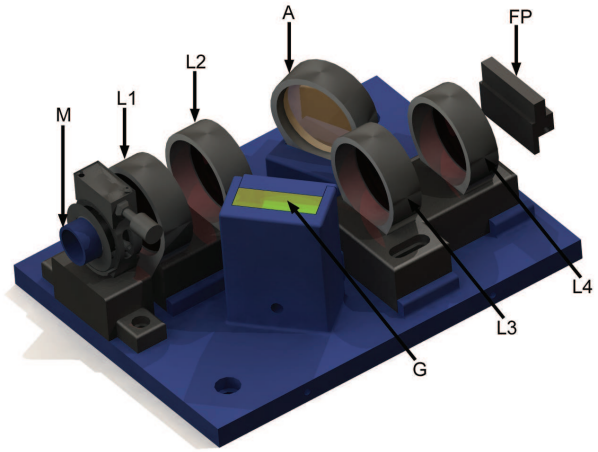

Fig. 1. 3D-Mechanical layout for the LWIR spectrometer.(M)Mask at input. (L1-L4)Lenses in the optical system. (A) Gold mirror. (G) Grating. (FP) Microbolometer focal plane array.

microbolometer array at the detector plane. Preliminary results from the prototype show that with higher quality instrumentation the static, aperture coded LWIR spectrometer can potentially provide a static, low cost and robust alternative to FTIR systems.

2. System design

We have designed and constructed a dispersive LWIR coded-aperture spectrometer with a spectral range of 9μm to 11μm. The experimental setup for the prototype is schematically shown in Fig. 1. The prototype consists of a coded-aperture at the input to a spectrometer layout with an uncooled microbolometer array at the detector plane.

Figure 2 describes the optical layout from the input source to the detector plane. The f/2 spectrometer has unity magnification from the source to the focal plane. The input aperture to the LWIR spectrometer is based on the row-doubled Hadamard matrix – a two dimensional array of transmissive and opaque openings explored in our previous work [6]. A shuffled version of the row-doubled Hadamard matrix is used to remove any spatial correlations within the row-doubled mask structure. This removes any coherent noise amplifcation complicating source recovery in multiplex systems. [11] The Hadamard matrix is electroformed as a rectangular pattern onto an 11mm nickel disc, 50μm thick. Each feature (a transmissive or opaque region) on the mask is 30μm square (see Fig. 3). For our LWIR system, the mask feature size is three times the size of a microbolometer pixel. Two dead rows, d, are added to each of the three rows in the code mapped onto the detector plane. The dead rows compensate for vertical misalignments and blurring caused by the optical system. A dead row is the size of a single mask element or 30μm in the LWIR prototype. Without dead rows, any vertical alignment would require precision down to about a fraction of the pixel size. The height and width of the mask is 3.54mm x 1.08mm (see Fig. 3) as defined by

$$M_H = 2nfp + (2n-1)dp \tag{1}$$

$$M_W = npf, \tag{2}$$

#78809 - $15.00 USD Received 10 Jan 2007; revised 20 Apr 2007; accepted 23 Apr 2007; published 25 Apr 2007

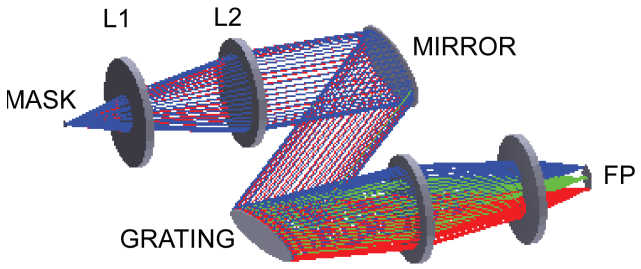

Fig. 2. Optical design layout for the LWIR spectrometer.

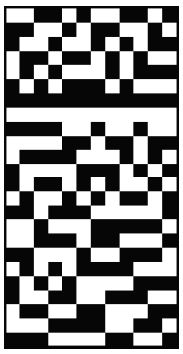

Fig. 3. Hadamard mask N=12.

where M_H is the mask height, M_W is the mask width, n is the order of the row-doubled Hadamard matrix(RHD), f is the number of pixels per mask element, p is the pixel size and d is the number of dead rows used in the design of the mask. The row-doubled mask is 50% transmissive resulting in a total open area of 1.1664mm^2, as defined by

$$M_{OA} = \frac{(2npf)(npf)}{2}, \tag{3}$$

where M_{OA} represents the mask open area. In comparison to the aperture-coded mask, a slit of exact width to the pixel size on the detector plane with a height of about 3.67mm provided a total open area of 0.1101mm^2. The total open area of the mask, while incurring about an 40% loss from dead rows in the configuration, yields a theoretical gain by a factor of ten compared to the open area of a slit. The theoretical throughput, however, for a row-doubled Hadamard matrix in comparison to a slit is $n/2$, where n is the order of the matrix. It has been shown in our previous work that the actual gain in throughput as the order of the RDH Hadamard matrix increases is about $n/4$. [6]

For durability, the nickel disc is sandwiched between two zinc selenide windows that are transmissive in the 9μm-11μm spectral range. All of the lenses (L1-L4) in Fig. 2 are 1 inch germanium, plano-convex lenses from *Janos*. Light directed through lenses L1 and L2 is reflected by a 1 inch gold plated mirror onto a grating. The grating has a groove density of 60 lines/mm with a clear aperture of 25mm square The grating is blazed for a 10μm center wavelength. Light dispersed after the grating is brought to a focus by a pair of germanium lenses

#78809 - $15.00 USD Received 10 Jan 2007; revised 20 Apr 2007; accepted 23 Apr 2007; published 25 Apr 2007

(L3 and L4) at the detector plane. The resolution of the LWIR system is limited by both the feature size and the spot size at the detector plane. Resolution is determined by the root-mean-square error calculation and linear dispersion, $d\lambda/dx$. The root-mean-square error calculation is defined by the feature size (Δf), the pixel size (Δs) and the spot size (Δr) in

$$\Gamma_\lambda = [\Delta f^2 + \Delta s^2 + \Delta r^2]^{1/2}. \tag{4}$$

The resolution of our prototype is about 81.979*nm*. However, the metric of interest for emission spectroscopy is resolution in wavenumbers. For our prototype the resolution for our spectral band of interest in wavenumbers or inverse centimeters is 8cm^{-1}.

Emission infrared spectra are recorded on an uncooled amorphous silicon microbolometer array. The microbolometer array is 160×120 pixels with a 30 μm square pitch. Based on the mask dimensions previously mentioned, the overall mask height approximately matches that of the focal plane (3.6mm). The microbolometer used in this prototype is a low resolution, low fidelity instrument with a thermal sensitivity of $\leq$ 50mK and a spectral range of 7 μm to 14 μm. A signal is measured at the detector plane as a direct measurement of temperature from the source at the input aperture to the spectrometer. The detector's pixels are temperature sensitive. Temperature variations from the source result in linear resistance changes on the detector plane. [12] The microbolometer used in this LWIR prototype is an uncooled detector plane, making it less bulky. This, however, introduces noise not normally present in a cooled detector. A general noise model for the bolometer assumes *m* noise sources contributing to error for source recovery, where *m* represents a particular noise contribution at the detector plane. We assume that the noise sources are independent and follow a gaussian distribution. The standard deviation of the noise estimate is described by the model

$$\sigma_s = \left(\sum_{N=1}^{M} \sigma_N^2 \right)^{1/2}. \tag{5}$$

Noise sources at the bolometer include photon noise, Johnson noise and 1/f or flicker noise. Photon noise is normally Poisson distributed for weak signals. This type of noise consists of the random fluctuations in the arrival rate of photons. Photons arriving at the microbolometer are described by energy characterized by a specific frequency and related to heat incident on the detector plane. Photon noise can be considered for both signal and background cases. In our case, the tunable laser is not photon starved at the detector plane. Therefore, the Poisson distribution simplifies to a normal distribution for photon abundant cases. Johnson noise or thermal noise is characterized by the readout circuit within the microbolometer. With an increase in temperature, random motion of electrons within the circuit increase, generating a noise voltage at the resistor leads. [13] Flicker noise (1/f) is also generated by the internal circuit of the microbolometer. Electrical conductance within circuits fluctuate due to imperfections within the material used to manufacture a resistor. These fluctuations have a noise power spectrum associated with them that decrease with frequency, as the name suggests. [10] In summary, the noise can be quantified for the photon noise contribution and complete noise estimate using

$$\begin{aligned} \sigma_p &= \left(\sigma_t^2 + \sigma_b^2\right)^{1/2} \\ \sigma_c &= \left(\sigma_j^2 + \sigma_f^2\right)^{1/2} \\ \sigma_s &= \left(\sigma_p^2 + \sigma_c^2 + \sigma_k^2\right)^{1/2}. \end{aligned} \tag{6}$$

The noise contributions defined in Eq. 6 correspond to photon noise; σ_p, target noise; σ_t, background noise; σ_b, the circuit noise; σ_c, Johnson noise; σ_j, 1/f noise; σ_f and pattern noise; σ_k. Noise in the uncooled microbolometer setup is primarily dominated by photon noise related to the background noise at the detector plane and pattern noise at the detector plane.

#78809 - $15.00 USD Received 10 Jan 2007; revised 20 Apr 2007; accepted 23 Apr 2007; published 25 Apr 2007

3. LWIR source reconstruction

3.1. Source profile at the detector plane

At the detector plane, the intensity detected by a dispersive spectrometer is measured by a convolution between the source and the input aperture to the spectrometer.

$$I(x',y') = \int\int\int H(x,x',y,y';\lambda)T(x,y)S(x,y;\lambda)d\lambda\,dxdy \tag{7}$$

Eq. 7 includes a propagation kernel, $H(x,x',y,y';\lambda)$, for the optical field through the spectrometer; a transmission function, $T(x,y)$, describing the input aperture to the spectrometer and a spectral density, $S(x,y;\lambda)$, describing the source being analyzed at position x and y. A reference frame located in the detector plane is denoted as (x',y'), while a reference frame at the input is described by (x,y). In the study of spectroscopy systems, translation is made in the lambda and x-axis, while the y-axis remains constant. For a dispersive spectrometer, the convolution between the input spectrum and the input aperture must take into consideration linear dispersion,(α), effects by the grating given a center wavelength (λ). The propagation kernel, as a result, takes the form of $H(x,y;\lambda)$ = δ(y-y')δ(x-(x'+α(λ-λ_c))), where δ is the dirac delta function. Linear dispersion from a grating is described by

$$\alpha = \frac{dx}{d\lambda} = \frac{mf}{\Lambda\cos(\theta_R.)} \tag{8}$$

Here, m is the diffraction order of the grating, f is the output focal length to the detector, Λ is the grating period, and θ_R is the angle of diffraction. After substituting the propagation kernel into Eq. 7, assuming the source is located at $x = 0$ and computing the integrals over λ and the y-direction Eq. 7 simplifies to:

$$I(x',y') = \int T(x,y')S(x,y';\frac{x-x'}{\alpha}+\lambda_c)dx \tag{9}$$

Commonly, in slit based systems, the slit width is the size of a square pixel on the detector plane. The slit width is then the smallest resolvable feature on the detector plane. As a result, the transmission function for the input aperture of slit-based dispersive systems can be approximated by a delta function. The intensity profile recorded on the detector plane considering the assumptions stated for the mask is:

$$I(x',y') = S(0,y;\lambda_c - \frac{x'}{\alpha}) \tag{10}$$

3.2. The reconstruction approach

Reconstruction of a source from a slit based dispersive instrument is quite simple. Figure 4 details the procedure followed for spectral source reconstruction. A slit of comparable width and height to the microbolometer pitch and detector height is detected at the focal plane. Row summation from data captured at the focal plane is summed for adequate reconstruction of the source.

While the transmission function for a slit based system can be approximated by a delta function, heuristically a family of functions have been explored for the transmission function, T(x,y), in coded-aperture based systems. [6] The LWIR prototype uses a row-doubled Hadamard matrix as previously noted. Using the two dimensional Hadamard matrix provides a better conditioned matrix for inversion. The mask is considered from an independent column code perspective where the input mask provides linear combinations of spectral components

#78809 - $15.00 USD Received 10 Jan 2007; revised 20 Apr 2007; accepted 23 Apr 2007; published 25 Apr 2007

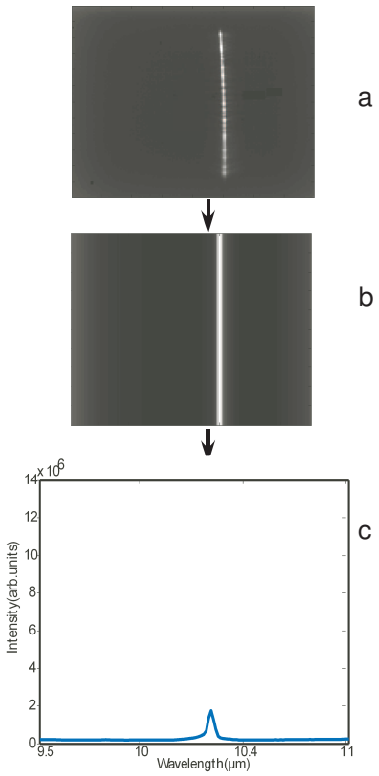

Fig. 4. Reconstruction procedure for a slit system.(a) Microbolometer raw image of a CO_2 laser emission spectrum at the focal plane. (b) Microbolometer image after binning the rows. (c) Reconstructed emission spectrum of a CO_2 laser.

that map onto known positions at the focal plane. Since the intensity profile measured is a convolution between the spectral density of the source and the row-doubled Hadamard code, adequate deconvolution techniques or inversion methods must be performed for source retrieval.

Figure 5 describes the reconstruction technique used for an aperture code inversion. For the mask based system, a convolution between the source and the mask is detected at the focal plane. After the image is captured at the focal plane, rows are binned to account for the 3:1 pixel to mask ratio (see Fig. 5(b1). A nonnegative least squares (NNLS) iterative algorithm is used to invert the binned data captured by the focal plane. [14] Data processing with the algorithm should conserve total number of counts detected at the focal plane. The row-doubled Hadamard matrix is first divided by the order of the mask to account for photon conservation. Then the matrix is used as an input to the NNLS algorithm for data inversion. The NNLS algorithm inverts the data column-by-column and provides spectral estimates of the source row-by-row as seen in Fig. 5(c). The algorithm is a least squares optimization technique with a nonnegativity constraint applied to the transformation matrix, E, and data vector, f, obtained at the focal plane of the instrument. A model for the nonnegative least squares problem is defined by

$$Minimize \ \ \|Ex - f\| \quad x \geq 0 \tag{11}$$

In Eq. 11, x represents the estimate for the signal of interest. Specific details regarding the algorithm have been defined by Hanson and Lawson. [14] The spectral estimates obtained from the

#78809 - $15.00 USD Received 10 Jan 2007; revised 20 Apr 2007; accepted 23 Apr 2007; published 25 Apr 2007

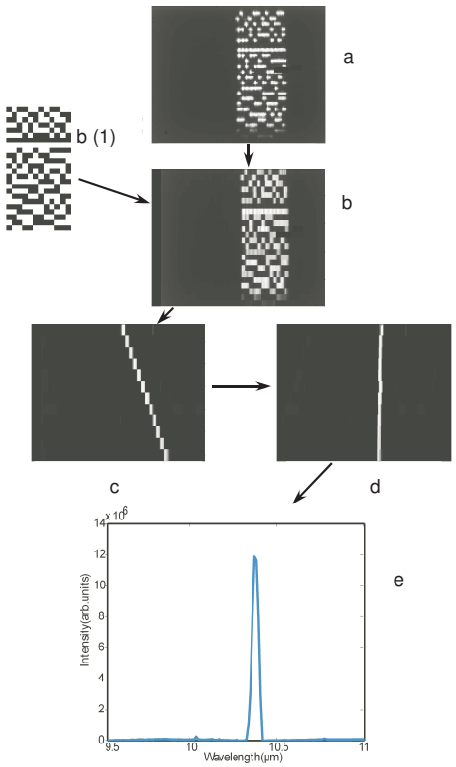

Fig. 5. Reconstruction procedure for an aperture-coded system. (a) Microbolometer raw image of a CO_2 laser emission spectrum. (b) Microbolometer data binned by rows. (b1)Image of a row-doubled Hadamard matrix. (c) Spectral estimates shown after a column inversion using the NNLS algorithm is applied to the binned data. (d) Spectral estimates are aligned for row summation. (e) Spectral reconstruction of the CO_2 source after row summation.

algorithm are then aligned by computing the correlation maximum between individual spectral estimates and a single reference spectral estimate. A sum is then taken over the aligned spectral estimates for adequate source recovery. After data processing, the spectrum of the source is plotted versus a calibrated x-axis.

4. Experimental results

Infrared emission spectra from a tunable CO_2 laser are recorded at the focal plane of a dispersive spectrometer. Results from both a slit and a mask are presented and compared.

A spatially extended, tunable CO_2 laser beam illuminates the mask at the input aperture of our prototype LWIR dispersive spectrometer. Photon flux collected through the mask and incident on the detector plane is wavelength dependent. The photon flux, Ψ_K, at the mask was calculated at the wavelength, λ, 10.35μm to be $3.75\times10^{16} photons/s$. The photon flux was found using

$$\Psi_K = \lambda P_\lambda \left(\frac{E}{hc}\right). \tag{12}$$

with $hc = 1.9864 \times 10^{-19} J\ \mu m$. In Eq. 12, h is planck's constant, c is the speed of light, E is

#78809 - $15.00 USD Received 10 Jan 2007; revised 20 Apr 2007; accepted 23 Apr 2007; published 25 Apr 2007

equal to .004 Joules with a laser power of 120mW and a frame rate for the detector of 30Hz. The photon irradiance at the input to the spectrometer in a given beam diameter, D, of 24.914mm is $7.695 \times 10^{13} photons/mm^2 s$. The number of photons per second through the mask and incident on the detector plane is 6.611 x 10^{13} $photons/sec$ using

$$\frac{\Psi_K}{D} M_{OA}. \tag{13}$$

In Eq. 13, D is the beam diameter after propagation from the laser to the input aperture of the spectrometer using gaussian optics and M_{OA} is the open area on the mask. Since the uncooled microbolometer is a low fidelity focal plane, the system is detector-noise limited and not photon-noise limited. The low fidelity focal plane, by default, makes the focal plane detector-noise limited. Only an extremely weak source of comparable intensity to pattern noise and detector noise noticed at the detector plane would make the system photon-limited. Also, for multiplex systems a low mask order decreases photon-noise limitations, while maximizing the gain in using a Hadamard mask over a conventional setup with a slit. [11] For the LWIR prototype, a photon-abundant source is analyzed at the focal plane as a starting point to calibrate the x-axis. A photon abundant source was also used to analyze the strengths and limitations of the design. Averaging 100 images minimizes the thermal noise present at the detector plane. First, for a calibration measurement of the x-axis, 100 laser shots at each wavelength tested are averaged and reconstructed for both the slit and the mask. The averaged images are shown in Fig. 6. Reconstructed multi-spectral data provided a framework for a polyfit and interpolation procedure for wavelength calibration. A calibrated wavelength axis was created for both the slit and the mask using the procedure above. Fig. 6 displays the multi-spectral data for both the slit and the mask.

5. SNR comparison

Spectral reconstructions between the slit and mask were compared. For adequate comparison the signal-to-noise ratios (SNR) between the slit and the mask were compared at various wavelengths. SNR may be defined in different ways. We have defined SNR by

$$SNR = \frac{I_M(\lambda) - \bar{N}}{\sigma_N}. \tag{14}$$

I_M is found by obtaining the maximum intensity value as a function of wavelength in the reconstructed image. To obtain the signal, the maximum intensity value is subtracted from an average, $\bar{N}$, "flat" region in the image classified as the noise floor. Noise is estimated by calculating the standard deviation, σ_N, of a selected noise floor region. Data points collected for the noise region at each wavelength were collected over the same number of points for adequate comparison. Data obtained from three wavelengths using the tunable CO_2 laser were compared based on the above metrics. Results are shown in Fig. 7. In theory, the expected SNR gain using the mask over the slit should be equal to the square root of the throughput. Recall that for a row-doubled Hadamard mask, the throughput is measured by N/2, where N is the order of the matrix being used. [6] Therefore, the theoretical limit for the SNR gain using an order N=12 mask yields a 2.45 gain. An experimental gain of 1.97 was measured at 9.673μm, a gain of 1.61 was measured at 10.247μm, 0.84 at 10.349μm, 2.17 at 10.696μm and 0.597 at 10.764μm. In comparison to the theoretical limit for gain of 2.44, data collected for the wavelengths mentioned are close in value. Some smaller SNR gain values can be attributed to the variation of signal strength when reconfiguring the setup for the mask or slit. The tunable laser drifted at times when tuning to a different wavelength. More importantly, a change in wavelength does

#78809 - $15.00 USD Received 10 Jan 2007; revised 20 Apr 2007; accepted 23 Apr 2007; published 25 Apr 2007

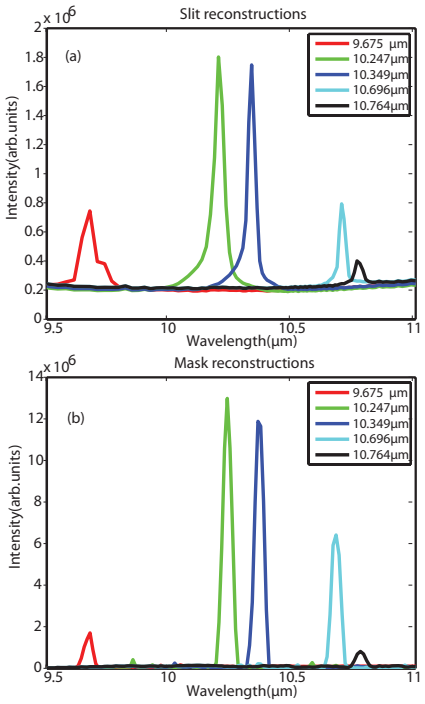

Fig. 6. Slit (a) and Mask (b) reconstructions for calibration of the x-axis.

not correspond to a linear increase or decrease in laser power. This is illustrated when looking at the relative peak heights for the various data points for each wavelength analyzed in Fig. 7.

Results from the aperture-coded LWIR prototype reveal an increase in SNR from a slit-based dispersive system, thus providing a solution over slit-based spectrometers for the spectral region of interest.

6. Conclusion

The design and construction of a LWIR coded-aperture spectrometer have been presented. While absorption spectroscopy measurements were not reported, the ideas summarized in this document can be extended for measurements in the LWIR for chemical detection and analysis.

An extended source from a tunable CO_2 laser illuminates the coded-aperture at the input to the LWIR prototype as a proof of concept. It is, then, sent through the spectrometer and detected by an uncooled microbolometer array. Comparison between a slit-based and aperture-coded spectrometer is made. While experimental results fall short of the theoretical gain, results show that the SNR of the mask-based spectrometer is increased by a factor of two. Several improvements can be made to the system to increase the sensitivity, allowing the detection of weaker sources such as aerosols or chemicals. Some of these improvements include the use of higher order masks, a more robust mechanical design and a higher fidelity microbolometer.

Typically, in the LWIR region, FTIR systems are used for chemical detection. FTIR systems are photon-efficient, but typically contain movable parts that increase the cost of the system and increase data acquisition times. Dispersive systems exist, but lack the photon-efficiency obtained with FTIR systems. The implementation of an aperture-coded dispersive instrument yields both a throughput and multiplex advantage similar to that of an FTIR system. The proof-

#78809 - $15.00 USD Received 10 Jan 2007; revised 20 Apr 2007; accepted 23 Apr 2007; published 25 Apr 2007

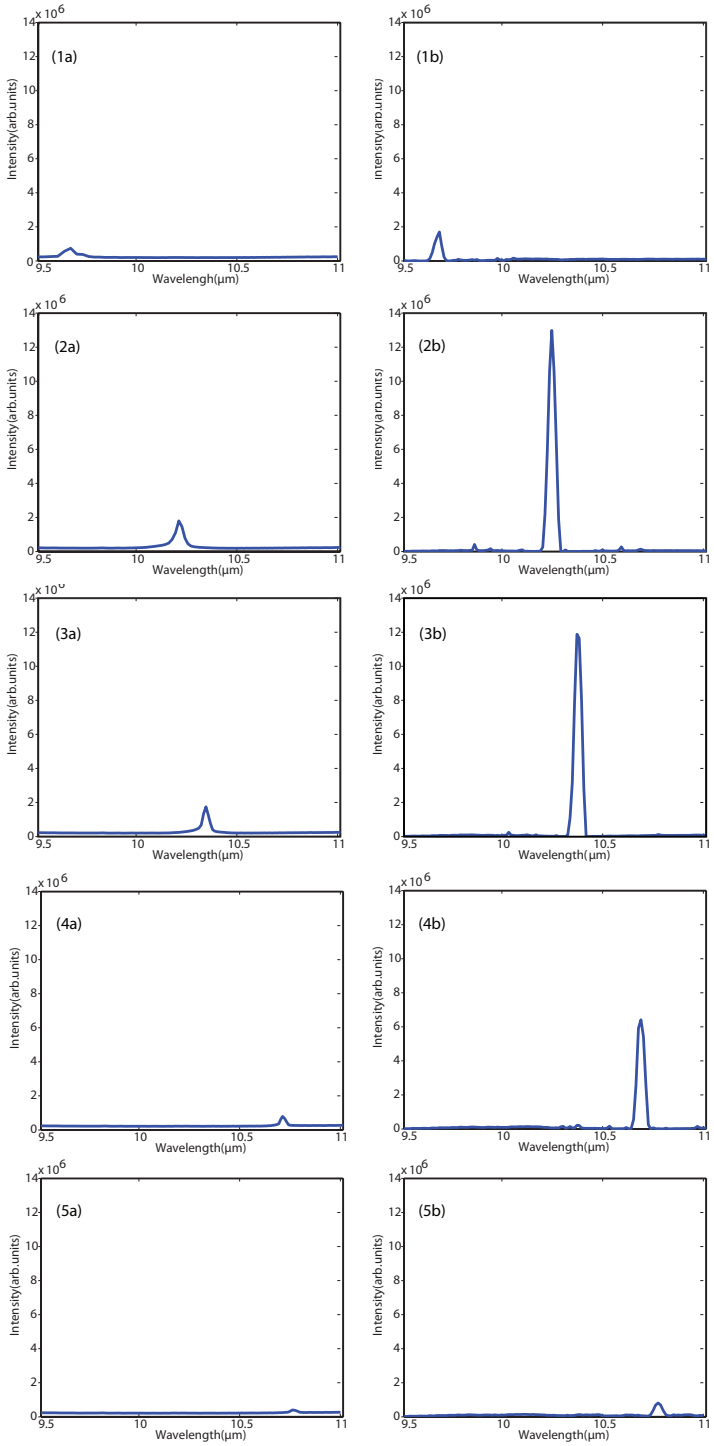

Fig. 7. Spectral reconstruction of a slit (left column) and mask (right column) for SNR comparison. Reconstructed plot are shown at wavelengths (1) 9.673 μm, (2) 10.247 μm (3) 10.349 μm, (4) 10.696 μm and (5) 10.764 μm.

#78809 - $15.00 USD Received 10 Jan 2007; revised 20 Apr 2007; accepted 23 Apr 2007; published 25 Apr 2007

of-concept system outlined in this paper introduces ideas which could be extended as an alternative to FTIR systems without the need for movable parts.

#78809 - $15.00 USD Received 10 Jan 2007; revised 20 Apr 2007; accepted 23 Apr 2007; published 25 Apr 2007